Estimating Soil Salinity Using HISUI Hyperspectral Data in the Western Australian Wheatbelt

Emiko Ariyasu [1], Satomi Kakuta [1]

[1] Asia Air Survey Co. Ltd., 1-2-2 Manpukuji Asao-ku Kawasaki-shi Kanagawa, 215-0004 Japan
- emk.ariyasu@ajiko.co.jp, stm.kakuta@ajiko.co.jp

Keywords: Arid, Map, Electrical Conductivity, Salt-affected, SWIR, Remote sensing.

Abstract

Soil salinity, caused by natural and anthropogenic factors, significantly impacts agricultural productivity, ecosystems, and global biodiversity. To mitigate severe salinity levels, it is necessary to detect early the salt-affected land for implementing solutions, such as adequate irrigation and cultivation of salt-tolerant crops. Before launching spaceborne hyperspectral sensor, Hyperspectral Imager Suite, (HISUI) developed by Japanese Ministry of Economy Trade and Industry, Kobayashi et al. (2010 and 2013) developed methods utilizing airborne hyperspectral data from HyMap to estimate soil salinity in wheatbelt region of Western Australia as a previous study. This paper aims to assess the feasibility of estimating soil salinity with HISUI in the same study area, following the past approach. Also, the goal is to estimate low soil salinity levels as same as the past objectives. As a result, past approach could not be fully applied in spaceborne hyperspectral sensor, caused by atmospheric effect in SWIR region. However, absorption of soil salinity in SWIR regions could be detected by HISUI. In the soil index, the NDSI (Normalized Difference Soil Index) showed higher accuracy than the Soil Index (SI) developed in previous studies. Then, the lowest values of RMSE were less than 100 mS/m in NDSI. As a result, HISUI data could not leach to map soil salinity at lower levels in this study. However, it showed the potential to estimate it with higher accuracy using hyperspectral data.

1. Introduction

Soil salinity is a serious environmental hazard affecting agricultural productivity, ecosystem stability, and biodiversity across the world. Especially, it is happened more severe in arid and semi-arid regions of Africa, Asia, and Latin America (Hussain, 2019). The increase of soil salinity is triggered by both natural and human-induced causes, including inadequate irrigation techniques, excessive use of fertilizers, and land use changes (Kaya et al., 2022). As a result, the phenomenon leads to a decline in the yields of agricultural products because growth is hindered by the plants' inability to uptake water (Niu et al., 2019). One of the soil-affected regions is Western Australia, where salinity poses a significant threat to agricultural lands and natural ecosystems (Australian Bureau of Statistics, 2002). Salinity in non-irrigated areas, known as dryland salinity, remains a potential risk to 2.8 to 4.5 million hectares of highly productive, low-elevation or valley soils in the southwest region of Western Australia (George et al., 2005).

Remote sensing techniques show high potential to monitor soil salinity on a large scale. Consequently, research on soil salinity has increased by remote sensing worldwide (Sahbeni et al., 2023). These techniques utilize two main wavelength regions to detect soil salinity: visible-to-near-infrared (VNIR) and shortwave infrared (SWIR). Studies indicate that the SWIR region provides higher accuracy for estimating soil salinity compared to the VNIR region in multispectral satellite data from Sentinel-2 (Bannari et al., 2018). Also, Bannari et al. (2008) applied salt-affected agricultural land in Morocco by spaceborne EO-1. However, no previous studies have estimated soil salinity forcused on SWIR using spaceborne hyperspectral sensors in Western Australia.

Hyperspectral Imager Suite (HISUI) was a Japanese spaceborne hyperspectral imager launched on December 6, 2019, and deployed on the Japanese Experiment Module of the International Space Station (ISS). The past study developed a method to estimate soil salinity using the airborne hyperspectral sensor, HyMap, in the wheatbelt region of Western Australia (Infoserve Inc., 2013; Infoserve Inc., 2015; Kobayashi et al., 2010; Kobayashi et al., 2013). Their study applied airborne hyperspectral data to map soil salinity, even at lower levels. It was a goal to support for decision making to manage salt-affected land. The airborne hyperspectral data was acquired in Marchagee and Toolbin on February 18, 2010. The sensor, HyMap, consisted of 128 bands covering wavelengths from 440 nm to 2500 nm. The process is, at first, the data was processed for surface reflectance using MODTRAN-based atmospheric correction, AtComp, developed by CSIRO (Ong, 2014), and pseudo-reflectance to remove topographic effects and shadows. After that, the data was applied removal vegetation with SWIR region for the data. Afterwards, it was processed to select two bands combination from 1970 nm to 2130 nm for a key of soil salinity. Then, it was selected Soil Index (SI) composing the maximum values of R_{max} in denominator and estimate soil salinity, using 26 points of soil sample data. In this study, we explored the possibility of estimating soil salinity using the spaceborne HISUI hyperspectral sensor, following the methodology of the previous study. Then, it is a goal to estimate soil salinity even in lower level, such as values of less than 50 mS/m as same as the past study. In the process, vegetation impact for removal was assessed using the VNIR region instead of the SWIR region, considering that spectral patterns in the SWIR were absorbed by H_2O. The Soil-adjusted Vegetation Index (SAVI) was applied for comparison. After that, index was generated SI Normalized Difference Soil Index (NDSI) for comparison, which composed of the sum of 2 bands in denominator. Through the entire process, soil salinity was estimated using the following models:

Model 1: soil salinity map after atmospheric correction
Model 2: soil salinity map after pseudo-reflectance
Model 3: soil salinity map after vegetation removal applied by the process of VNIR region
Model 4: soil salinity after vegetation removal applied by SAVI

This contribution has been peer-reviewed. The double-blind peer-review was conducted on the basis of the full paper.
https://doi.org/10.5194/isprs-annals-X-4-2024-21-2024 | © Author(s) 2024. CC BY 4.0 License.

2. Materials

2.1 HISUI Hyperspectral Data

Hyperspectral Imager Suite (HISUI) was launched and mounted on the Japanese Experiment Module of the International Space Station. HISUI was developed by the Japanese Ministry of Economy, Trade and Industry. It is composed of 185 bands with two spectrometers in the VNIR and SWIR regions to cover wavelengths from 400 nm to 2500 nm (J-spacesystems, 2024; Tachikawa et al., 2012). The swath width is 20 km by 30 km, and the resolution was 20 m by 20 m. In this study, hyperspectral data was selected for the area (Latitude: -29.96952° to -30.318084°, Longitude: 116.00669° to 116.373315) acquired on November 7, 2021. The scene was partially including the past study area. The data was provided as an L1G level product, which is a geometrically corrected and orthorectified top-of-atmosphere spectral radiance product (J-spacesystems, 2024).

Sensor name	Hyperspectral Imager Suite (HISUI)
Launch date	December 6, 2019
Spatial resolution	20 m × 20 m
Wavelength	400 nm - 2500 nm VNIR: 400 nm - 970 nm SWIR: 900nm - 2500nm
Band number	185 (VNIR:57, SWIR:128)
Spectral resolution	VNIR: 10 nm SWIR: 12.5 nm
Data size	12 bits

Table 1. HISUI data specification

2.2 Study Site

The study site is located between Marchagee and Guyindi in the state of Western Australia, approximately 240 km north of the capital city, Perth (Figure 1). The bioclimate is classified as Thermoxeric, indicating a predominantly dry to extra dry Mediterranean climate, characterized by cool to mild wet winters from April to September, and hot, dry summers from October to March (Beard, 1990). Geological reports from the government indicate that the region overlays the South West Terrane of the Yilgarn Craton, consisting of Archaean granitic rocks. These are primarily composed of monzogranite, with significant portions of gneiss, granulite, and migmatite. The soil types are sandy duplex soils and ironstone gravelly soils, along with loamy earths, loamy duplexes, sandy earths, deep sands, and wet soils (Tille, 2006). The area features naturally formed salt lakes (playas) from the Cainozoic era (George et al., 2006). In terms of land use, the region predominantly supports agricultural activities, with wheat and canola as the main crops. These crops typically reach their peak growth in August or September (Caccetta et al., 2022).

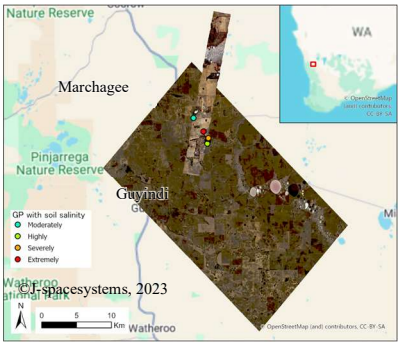

Figure 1. Location of the study and HISUI and HyMap data (HISUI : R=635 nm, G=545 nm, B=465 nm)

2.3 Field Measurements

Field measurements were conducted in October 2012 to collect soil samples and reflectance data for a previous study. Out of 70 collection points, soil samples from only 12 locations were covered by HISUI data. The field measurements included the sampling of electrical conductivity (EC) at a 1:5 soil-to-water ratio, a standard method for assessing soil salinity in Australia. The EC values recorded for this study were as follows: 41, 43, 59, 63, 65, 93, 100, 150, 170, 5,000, and 22,000 mS/m. According to classifications provided by the Government of Western Australia (2022), the soil samples were categorized based on $EC_{1:5}$ (w/v) loam values in mS/m. The salinity classes were defined as follows: “Moderately” for 5 samples with EC values ranging from 40 to 80 mS/m, “Highly” for 3 samples with EC values from 80 to 160 mS/m, “Severely” for 2 samples with EC values from 160 to 320 mS/m, and “Extremely” for 2 samples with EC values exceeding 320 mS/m.

3. Method

Following the process of the past report, this study was applied to estimate soil salinity and generate the map as shown in Figure 2 below.

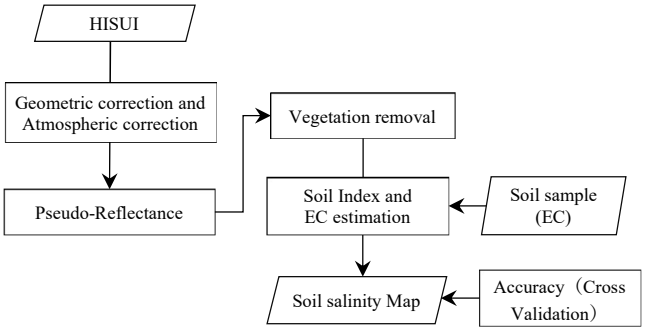

Figure 2. Process flow

3.1 Geometric Correction and Atmospheric Correction

The HISUI data was geometrically corrected within 1 pixel by referencing Sentinel-2 L2A, acquired on November 7, 2021. After that, HISUI data required to be converted to radiance ($W/m^2/sr/\mu m$). The radiance data was applied an atmospheric correction with Fast Line-of-Sight Atmospheric Analysis of Spectral Hypercube (FLAASH), which is a MODTRAN-4 based approach that is available in ENVI software. The atmospheric model was applied with Mid-Latitude Summer, and the aerosol model was selected Rural. Also, water retrieval was selected with 1135 nm of water absorption feature. The corrected data was multiplied by 10,000 to keep the integer unit.

3.2 Pseudo-reflectance

The past study processed pseudo-reflectance after atmospheric correction (Kobayashi et al., 2010). The pseudo-reflectance was applied to remove the effects of topographic features and shadows by normalizing the reflectance by square root of the sum from the reflectance of 185 bands squared.

$$PR_n = \frac{R_n}{\sqrt{\sum_{n=1}^{185} R_n^2}} \quad (1)$$

where R = reflectance
n = number of bands

3.3 Vegetation Removal

The data still contained vegetation in the area. To improve the estimation of soil salinity, it was conducted spectral unmixing of soils and vegetation. Based on the past study, pseudo reflectance of pure soil, R_{soil} is given by the following equation:

$$R_{soil} = \frac{OPR - X(VPR)}{1 + X} \quad (2)$$

where OPR = pseudo-reflectance including soils and vegetation
VPR = vegetation of pseudo-reflectance
X = impact of vegetation

VPR is average pseudo reflectance of the vegetation area found in the crop fields, except trees, which is not a target in this study. X is defined as the angle formed by the reflectance at 1114 nm, 1202 nm, and 1244 nm and derived from following equation:

$$\frac{(OPR_{1202} - VPR_{1202} * X) - (OPR_{1114} - VPR_{1114} * X)}{1202 - 1114} = \frac{(OPR_{1244} - VPR_{1244} * X) - (OPR_{1202} - VPR_{1202} * X)}{1244 - 1202} \quad (3)$$

At the angle formed by the three wavelengths, if the impact of vegetation is significant, it becomes an acute angle, and if it is low, it approaches the value of a straight line (180 degrees). Due to the area spreads the rest of cultivated products after harvesting and natural vegetation, which is salt-tolerant shrub and grass, such as Chenopodiaceas, vegetation characteristic, red-edge in their spectral pattern between red and NIR are not observed (Ben-Dor et al., 2008). Therefore, vegetation impact was estimated by using spectral absorption of water in vegetation around 1200 nm of SWIR bands. However, in HISUI data, it was found that the reflectance at 1114 nm and 1202 nm was affected by absorption of H_2O in air, so it was not the expected indicator. Figure 3 shows the spectra of green vegetation, soil (unpaved road), and dry vegetation sampled from the HISUI pseudo reflectance image. In Figure 3, the wavelengths at which the angles formed by the three wavelengths are acute angles are 565 nm, 685 nm, and 745 nm, which are not affected by the atmosphere and are only green vegetation. Thus, in this study, the three wavelengths of 565 nm, 685 nm, and 745 nm of VNIR bands were substituted for three wavelengths around 1200 nm in eq. 3.

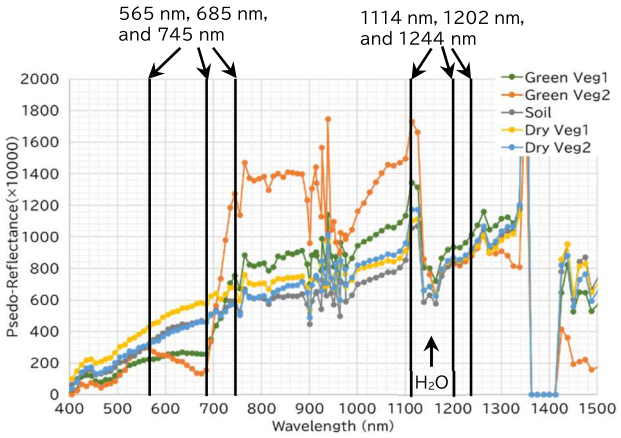

Figure 3. Spectra of green vegetation, soil (unpaved road), and dry vegetation sampled from HISUI pseudo reflectance image.

In addition to the vegetation impact indicator, this study also considered, for comparative purposes, the use of SAVI (Soil Adjust Vegetation Index) (Huete, 1988), which were calculated using reflectance corrected for atmospheric correction.

$$SAVI = \frac{(NIR - Red)}{(NIR + Red + L)}(1 + L) \quad (4)$$

where NIR = reflectance at 835 nm
Red = reflectance at 655 nm,
L = amount of green vegetation cover

SAVI was selected among variable vegetation indices because it corrects the effect of soil background brightness for lower amount of vegetation. The angle X derived from VNIR and SAVI were linearly transformed to range from 0 to 1, encompassing their minimum to maximum values, and were subsequently utilized as indicators of vegetation impact in experimental trials.

3.4 Soil index and EC Estimation

The past study focused on the water absorption feature from 1970 nm to 2130 nm, based on Whiting et al. on 2003. Also, this area was known the absorption feature observed near 2200 nm with soil moisture (Mouazen et al., 2006). In the past study, soil index was calculated as the difference in reflectance between the two bands selected from 1970 nm to 2130 nm and divided by the maximum reflectance of each soil spectra to estimate EC values.

$$SI = \frac{(R_{SWIR1} - R_{SWIR2})}{(R_{max})} \quad (5)$$

where SI = Soil index
R_{SWIR1}, R_{SWIR2} = reflectance at SWIR band from 1950 nm to 2100 nm
R_{max}= the maximum reflectance of each soil spectra from 1950 nm to 2100 nm

Band combination of R_{SWIR1} and R_{SWIR2} were selected by the highest coefficient of determination performing through correlation analysis among the soil index and EC values.

Soil spectral signature effects shows soil information about organic matter content, moisture, mineral composition, color bright, roughness. Bannari et al. (2008) denotes spectral properties of the soil salinity are detectable in the SWIR region and proposed NDSI (Normalized Differential Soil Index).

$$NDSI = \frac{(R_{SWIR1} - R_{SWIR2})}{(R_{SWIR1} + R_{SWIR2})} \quad (6)$$

For comparison, the two soil indices were applied to the below EC equation with 12 EC values:

$$EC = EXP((Soil\ index + a)/b) \quad (7)$$

where a, b = model coefficient given by soil samples

3.5 Accuracy

For accuracy validation, a cross-validation was employed by Leave-one-out method. It evaluates one sites of the remaining EC values and iterated through the entire dataset. This procedure was iterated 12 times, sequentially rotating the data so each site was used once as the validation set. Subsequently, the Root Mean Square Error (RMSE) was calculated using the following formula:

$$RMSE = \sqrt{\frac{1}{n}\sum_{i=0}^{n-1}(y_i - \hat{y}_i)^2} \quad (8)$$

where $\hat{y}_i$ = the predicted value of the sample
y_i = the measured value

4. Result and Discussion

After processing the HISUI data with atmospheric correction using FLAASH in an urban local area, the HISUI data indicates the spectral reflectance pattern in the SWIR region from 1800 nm to 2500 nm in Figure 4. It shows 12 points of soil sample data were categorized with soil salinity class. All spectra show absorption in the negative peak from 1800 nm to 1950 nm and at 2025nm by atmospheric molecules, which was not shown by airborne sensor, HyMap at the past study, because image in HyMap is not affected by the atmosphere like HISUI due to its low altitude of observation. Also, it shows absorption from 1950 nm to 2000 nm, which is denoted that soil salinity related with liquid absorption because it contains liquid water molecules in soils in the past study.

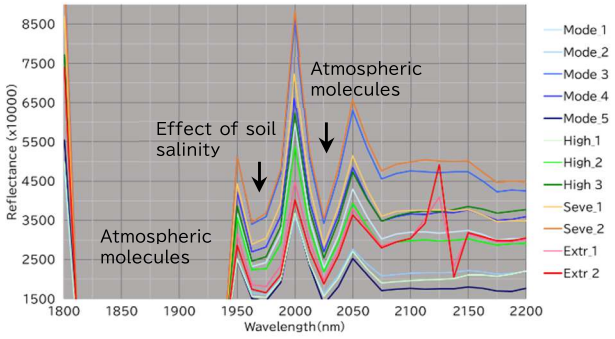

Figure 4. Spectral pattern between 1800 nm to 2200 nm

Following the process of pseudo-reflectance and vegetation removal, the two bands were selected by the highest determination coefficient, R^2, from the range of 1950 nm to 2000 nm, with avoiding spectral absorption caused from CO_2 from 2000 nm to 2050 nm in HISUI. After selecting the two bands, the soil index was assigned in exponential model. In fact, linear regression also tested, but it was not adapted in that the coefficient determination was low. Figure 5 shows (a) a heat map of R^2 among the soil index and EC values. Blackish zone from 200 nm to 2100 nm was out of range for spectral absorption. (b) indicates an exponential regression model for soil salinity estimation by the soil index. The soil index was computed from eq. 5 by applying pseudo-reflectance after vegetation removal with the impact indicator of the angle formed by the three wavelengths of VNIR.

	1950	1963	1975	1988	2000	2013	2025	2038	2050	2063	2075	2088	2100
1950													
1963	32.2%												
1975	0.2%	33.3%											
1988	17.6%	77.1%	59.3%										
2000	72.6%	77.4%	59.5%	58.7%									
2013	27.7%	3.8%	3.4%	34.8%	85.8%								
2025	46.5%	40.0%	69.3%	68.7%	67.4%	28.8%							
2038	58.2%	51.0%	68.6%	70.1%	70.5%	42.9%	50.2%						
2050	75.1%	65.3%	70.6%	74.9%	78.7%	66.6%	53.5%	49.8%					
2063	78.4%	71.7%	75.7%	78.1%	80.3%	71.7%	68.8%	73.8%	86.8%				
2075	75.5%	70.8%	76.4%	77.2%	77.8%	68.1%	75.2%	82.1%	66.3%	20.4%			
2088	77.9%	73.7%	78.1%	78.9%	79.4%	71.8%	77.6%	83.6%	79.5%	69.0%	86.1%		
2100	78.8%	74.6%	78.5%	79.2%	79.9%	73.3%	78.4%	83.7%	81.8%	76.6%	85.6%	82.0%	

(a)

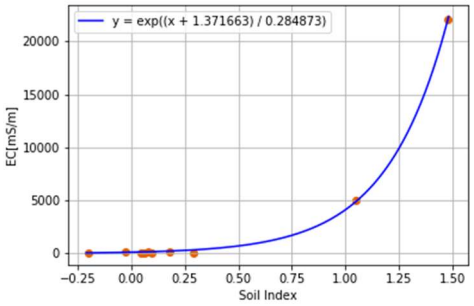

(b)

Figure 5. (a) Heat map of determination coefficient, R^2, among the soil index and EC values. (b) Exponential regression model for soil salinity estimation.

In this study, eight models were developed to estimate soil salinity, following the order of the processing flow and types of soil indices. Table 2 indicates all models and their coefficients of determination. Model 1 employed reflectance after atmospheric correction. Model 2 applied pseudo-reflectance. Model 3 and 4 both involved pseudo-reflectance after vegetation removal, but for Model 3, the vegetation impact indicator was estimated by the angle formed by the three wavelengths of VNIR, and for Model 4, the indicator was estimated by SAVI. Model A indicates SI as the soil index from eq. 5 and Model B refers to NDSI from eq. 6. As a result, these models indicated high coefficient values of EC on both of SI and NDSI. Among all models, the combination of 1987.65 nm and 2062.585 nm was selected in most cases. Therefore, the combination of those bands was found to be important in understanding the soil salinity by using HISUI.

	Model of soil salinity estimation	R^2
Model 1A	$EC = EXP\left(\frac{SI - 0.007406}{0.037989}\right)$ $SI = \frac{(R_{2062.585} - R_{1975.155})}{R_{max}}$	0.999679
Model 2A	$EC = EXP\left(\frac{SI - 0.002996}{0.038506}\right)$ $SI = \frac{(R_{2062.585} - R_{1975.155})}{R_{max}}$	0.999626
Model 3A	$EC = EXP\left(\frac{SI + 1.371663}{0.284873}\right)$ $SI = \frac{(R_{2100.055} - R_{1987.645})}{R_{max}}$	0.999666
Model 4A	$EC = EXP\left(\frac{SI + 0.883086}{0.165523}\right)$ $SI = \frac{(R_{2100.055} - R_{1987.645})}{R_{max}}$	0.998064
Model 1B	$EC = EXP\left(\frac{NDSI + 0.039816}{0.024554}\right)$ $NDSI = \frac{(R_{2062.585} - R_{1987.645})}{(R_{2062.585} + R_{1987.645})}$	0.999869
Model 2B	$EC = EXP\left(\frac{NDSI + 0.042622}{0.024878}\right)$ $NDSI = \frac{(R_{2062.585} - R_{1987.645})}{(R_{2062.585} + R_{1987.645})}$	0.999863

Model 3B	$EC = EXP\left(\frac{NDSI + 8.651934}{1.337036}\right)$ $NDSI = \frac{(R_{2062.585} - R_{1987.645})}{(R_{2062.585} + R_{1987.645})}$	0.964301
Model 4B	$EC = EXP\left(\frac{NDSI + 0.666613}{0.127264}\right)$ $NDSI = \frac{(R_{2062.585} - R_{1987.645})}{(R_{2062.585} + R_{1987.645})}$	0.996503

Table 2. Estimated models and Coefficient Determination

As a result, every model was mapped using the same legend: blue for the lowest EC values, gradually changing to green, yellow, and red for the highest EC values. Models 1 and 2, which did not apply vegetation removal, showed variable color ranges in their soil salinity maps. The east side of salt lakes where are accumulated salt over the surface on the ground are higher reflectance in True color image and estimated-EC values indicates more than 2,000 mS/m. The middle area of map shown cultivated area is mostly less than 10 mS/m. In the case of Model 3, which was applied vegetation removal by the process of VNIR region, the Salt Lake exhibits around 650 mS/m to 700 mS/m, which underestimated the area. Additionally, soil salinity in Model 3 ranged from approximately 600 to 700 mS/m across the entire dataset. Model 4, which applied vegetation removal using SAVI, showed EC values of approximately 200 to 300 mS/m, with the salt lake showing higher EC values. Models A and B, which applied different types of soil indices, did not show significant differences. Figure 6 shows soil salinity maps in Model 1B and 3A where Model 1B is the model with the highest coefficient determination, while Model 3A is the model after whole process. Also, Figure 6 (d) shows a color-composited image created using three bands related to soil salinity (R: 2062.585 nm, G: 1987.645 nm, B: 1975.155 nm). In the soil salinity color-composited image, areas affected by soil salinity are shown in reddish colors.

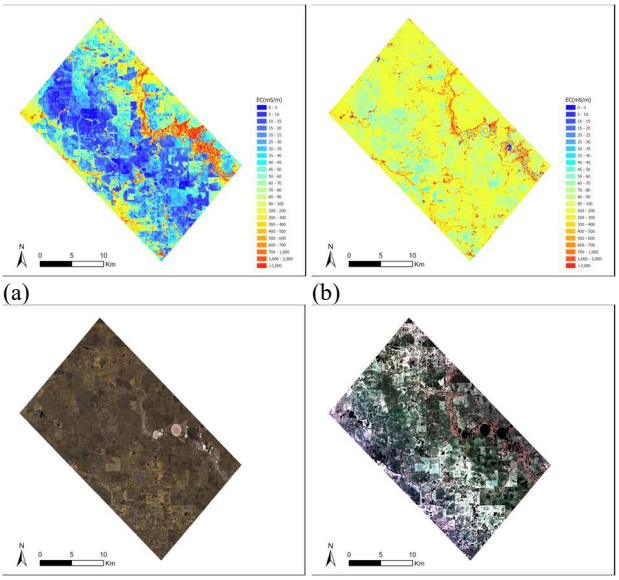

(a) (b) (c) (d)

Figure 6. Examples of soil salinity maps. (a) Soil salinity map in Model 1B, (b) Soil salinity map in Model 3A, (c) Atmospheric corrected image (R=635 nm, G=545 nm, B=465 nm), (d) Soil salinity color-composited image (R=2062.585 nm, G=1987.645 nm, B=1975.155 nm)

Figure 7 shows an enlarged soil salinity map in Model 1B adjusted the range of soil salinity referred to soil salinity class provided by the Government of Western Australia (2022) on the left figure, (a) and the soil salinity color-composited image on the right figure, (b). These both images exhibit the same trend. When the soil salinity map shows ‘Severely’ (in orange) and ‘Extremely’ (in red), in color-composited image, the effects of soil salinity are indicated by area appearing in red color. In soil salinity map, when Google Earth was used to see the ground in detail, it has been observed that areas covered with dense vegetation, such as trees, indicated as location with high soil salinity.

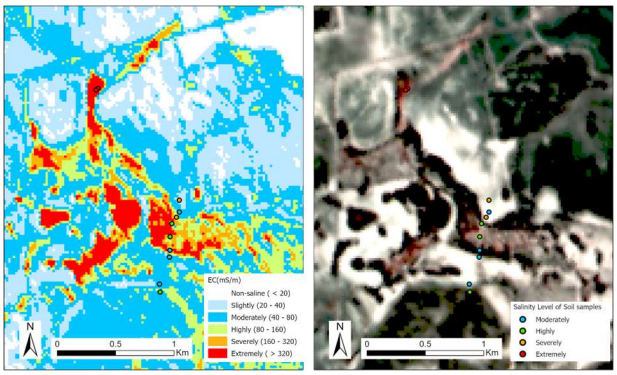

(a) (b)

Figure 7. Evaluation of soil salinity map. (a) Adjusted color level with salinity class along Western Australia, (b) Soil salinity color-composited image (R=2062.585nm, G=1987.645nm, B=1975.155nm)

Table 3 and Table 4 listed the true EC values and the estimation by each model. Each model was applied using cross-validation to validate the EC values of ground data. Table 3 for SI presented RMSE for the entire dataset ranging from 3,000 to 20,000 mS/m. However, when the dataset was filtered less than 1,000 mS/m, the values of RMSE was dramatically declined up to the value from 117 to 270. Table 4 for NDSI presented RMSE for the entire dataset were variable. However, when the dataset was less than 1,000 mS/m, the lowest RMSE, 77 mS/m, presented in both tables. Compared with each model, Table 3 indicated lowest RMSE were Model 3A for the entire dataset and Model 1A for less than 1,000 mS/m and Table 4 presented Model 1B at both datasets. In the method of previous study is similar to Model 3A, the method was shown the lowest RMSE for the entire dataset. However, this study case was shown the lowest RMSE for less than 1,000 mS/m dataset in NDSI.

		Estimation			
		Model 1A	Model 2A	Model 3A	Model 4A
Truth (EC at soil sample)	41	139	146	155	265
	43	232	247	355	679
	59	163	173	149	259
	63	110	116	145	255
	65	85	91	61	122
	93	126	133	148	246
	100	152	162	174	300
	150	405	424	233	493
	170	73	77	112	178
	190	198	205	163	294
	5,000	3,857	3,765	3,861	2,623
	22,000	32,452	33,773	32,183	67,159
RMSE		3,037	3,419	2,960	13,057
RMSE (EC<1000)		117	126	120	270

Table 3. Cross Validation for SI (units: mS/m)

		Estimation			
		Model 1B	Model 2B	Model 3B	Model 4B
Truth (EC	41	58	61	737	342
	43	181	190	820	715

	59	67	71	734	347
	63	51	54	724	315
	65	33	35	582	249
	93	68	72	749	386
	100	77	82	751	402
	150	236	248	779	600
	170	29	31	695	252
	190	91	95	734	382
	5,000	4,669	4,589	324	2,248
	22,000	24,044	24,673	6.97E+09	92,092
RMSE		602	784	2.01E+09	20,252
RMSE(EC<1000)		77	79	6.38E+02	339

Table 4. Cross Validation for NDSI (units: mS/m)

5. Conclusion

Soil salinity is an escalating environmental concern that compromises agricultural productivity and ecosystems, especially in arid and semi-arid regions, including Western Australia. Remote sensing has proven to be an effective tool for monitoring and identifying current soil salinity levels. In the past study, they studied a method to estimate soil salinity using airborne hyperspectral data (Kobayashi et al., 2010; Kobayashi et al., 2013). This study followed their methodology in the same area, using spaceborne hyperspectral data from HISUI. Pseudo-reflectance was processed to remove topographic effects and shadows, and vegetation removal was applied using two methods (VNIR and SAVI). At the next, two band combination was searched from regions of SWIR region, and soil salinity map was generated with Soil Index in the past study and NDSI assigning the sum of two bands for comparison. For the validation, the lowest RMSE at both indices was indicated Model 1B, which generated soil salinity map after atmospheric correction in NDSI. It could estimate EC reaching 77 mS/m in RMSE if the dataset filtering EC values at less than 1,000 mS/m. Based on the RMSE values, soil salinity could not be estimated at the lower levels of soil salinity. However, it could detect the spectral feature for the absorption of soil salinity in the SWIR region. The previous study was applied with airborne hyperspectral data in the same region. As a result, it was different approach was the highest accuracy at HISUI data in fact that atmospheric effect from spaceborne and airborne sensor and acquisition date were different.

For improving the model, it is necessary to add more soil samples because the past study could estimate by the lower EC values of 26 soil samples. On the other hand, in this study, the model was created with 12 soil samples with an unbalanced range of EC values. If possible, it should have applied to add lower level of EC, such as “Slightly” class of EC, 20 – 40 mS/m and “Severely” class of EC, 160 – 320 mS/m. In fact, even though it could estimate the soil salinity, it is not enough to generate a more reliable model. In the next time, we would like to implement a same soil salinity method with abundant soil samples and try in different regions of salt-affected country and different spaceborne hyperspectral sensor. In recent years, spaceborne hyperspectral satellite with specifications comparable to HISUI have been launched. For example, the Indian Space Research Organization (ISRO) launched HySIS on November 29, 2018, covering wavelengths from 200 to 2400 nm with a spectral resolution of 10 nm (ISRO, 2018), the Agenzia Spaziale Italiana (ASI) launched PRISMA on March 22, 2019, covering wavelengths from 400 nm to 2505 nm with a spectral resolution of 12 nm (ASI, 2024), and, the German Aerospace Center (DLR) launched EnMap on April 1, 2022, observing over wavelength from 430 to 2450 nm with a spectral resolution of 10 nm in SWIR (DLR, 2022). This research will be useful to show spectral features of soil salinity using those above spaceborne hyperspectral data.

Acknowledgement

This study was conducted a part of the project, named “Application research for soil salinity” entrusted by J-spacesytems under the Ministry of Economy, Trade and Industry, Japan in FY2023.

References

Agenzia Spaziale Italiana (ASI), PRISMA., Hyperspectral satellite, capable of observing from the optical to the near infrared. asi.it/en/earth-science/prisma (20 May 2024)

Australian Bureau of Statistics, 2002. Salinity on Australian farms 2002, Bulletin 4615, Australian Bureau of Statistics, Canberra. agric.wa.gov.au/soil-salinity/dryland-salinity-western-australia-0 (20 March 2024)

Bannari, A., Guedon, A. M., El-Harti, A., Cherkaoui, F. Z., El-Ghmari, A., 2008. Characterization of slightly and moderately saline and sodic soils in irrigated agricultural land using simulated data of advanced land imaging (EO-1) sensor. *Communications in Soil Science and Plant Analysi*s, 39(19–20), 2795–2811. doi.org/10.1080/00103620802432717

Bannari, A., El-Harti, A., Bannari, R., Rhinane, H., 2018. Sentinel-MSI VNIR and SWIR Bands Sensitivity Analysis for Soil Salinity Discrimination in an Arid Landscape. *Remote Sensing*. 2018, 10(6), 855. doi.org/10.3390/rs10060855

Beard, J. S., 1990. *Plant life of Western Australia*. Kangaroo Press Pty Ltd, Kenthurst NSW.

Ben-Dor, E., Metternicht, G., Goldshleger, N., Mor, E., Mirlas, V., Basson, U., 2008. Review of Remote SensingBased Methods to Assess Soil Salinity. In: Metternichtand, G. and Zinck, A., Eds., *Remote Sensing of Soil Salinization Impact on Land Management*, CRC Press, Boca Raton, 377.

Caccetta, P. A., Simons, J., Furby, S., Wright, N., George, R., 2022. Mapping salt-affected land in the South-West of Western Australia using satellite remote sensing, CSIRO Report Number EP2022-0724, CSIRO, Australia.

German Aerospace Center (DLR), 2022. German satellite EnMAP launches successfully, dlr.de/en/latest/news/2022/02/ (10 May 2024)

Government of Western Australia, 2022. Measuring Soil Salinity, Department of Primary Industries and Regional Development's Agriculture and Food. agric.wa.gov.au/soil-salinity/measuring-soil-salinity (20 March 2024)

George, R. J., Kingwell, R., Hill-Tonkin, J., Nulsen, R., 2005. Salinity investment framework: Agricultural land and infrastructure. Resource management technical report 270. Department of Agriculture, Western Australia.

George, R., Clarke, J., English, P., 2006. Modern and palaeogeographic trends in the salinisation of the Western Australian Wheatbelt, ASEG Extended Abstracts, 2006:1, 1-22, doi.org/10.1071/ASEG2006ab049

Hussain, S., 2019. *Climate Change and Agriculture*, 1st ed.; IntechOpen: London, UK, 2019; 1-26. ISBN 978-1-78985-667-5

Huete, A., 1988. A soil-adjusted vegetation index (SAVI). *Remote Sensing of Environment* 25(3), 295-309.

Indian Space Research Organisation (ISRO), Department of Space. 2018. PSLV-C43 / HysIS Mission. isro.gov.in/ mission_PSLV_C43 (20 May 2024)

Infoserve Inc., 2013. Estimating Soil Salinity Using Hyperspectral Data in arid and Semi-arid Regions, FY2012 Research and Development of the Fundamental Technology for Next-generation Satellite Utilization. FY2012 Technical report. J-Spacesystems (*in Japanese*)

Infoserve Inc., 2015. Development of Mapping Techniques for Soil Salinity in the Arid and the Semiarid Regions Aiming at the Plactical Use of Hyperspectral Data, FY2014 Research and Development of the Fundamental Technology for Next-generation Satellite Utilization. FY2014 Technical report. J-Spacesystems (*in Japanese*)

J-spacesystems, HISUI-Hyperspectral Imager Suite, Instruments, Product Description, hisui.go.jp/en/product/index (1 March 2023)

Kaya, F., Schillaci, C., Keshavarzi, A., Başayiğit, L., 2022. Predictive Mapping of Electrical Conductivity and Assessment of Soil Salinity in a Western Türkiye Alluvial Plain. *Land* 11(12), 2148. doi.org/10.3390/land11122148

Kobayashi C., Kashimura O., Maruyama T., Oyanagi M.,, Lau I.C, Cudahy T., Wheaton B., Carter D., 2010. Method to reduce green and dry vegetation for soil mapping using hyperspectral data. *International Archives. Photogramm. and Remote Sens.,Spatial Inf. Sci.,* Commission VIII, WG VIII/5. doi.org/10.13140/2.1.1857.7289

Kobayashi, C., Lau, I., Wheaton, B., Cater, D., Bourke, L., Asada, N., Kashimura, O., Ong, C., and Cudahy, T., 2013. Estimating soil salinity using hyperspectral data in the Western Australian wheat belt. *International Geoscience and Remote Sens. Symposium,* doi.org/ 10.1109/IGARSS.2013.6723791

Mouazen, A., De Baerdemaeker, J., Ramon, H. 2006. Effect of wavelength range on the measurement accuracy of some selected soil constituents using visual-near infrared spectroscopy. *J. Near Infrared Spectrosc*, 14, 189–199. doi.org/10.1255/jnirs.614

Ong, C.C.H., 2014. Mapping and Monitoring. The Environmental Impacts of Mining Using Hyperspectral Data, Curtin University of Technology, 34.

Sahbeni, G., Ngabire, M., Musyimi, K. P, and Székely, B., 2023. Challenges and Opportunities in Remote Sensing for Soil Salinization Mapping and Monitoring: A Review. *Remote Sensing*, 15, 2540. doi.org/10.3390/rs15102540

Tachikawa, T., Kashimura, O., Tani, J., Iwasaki, A., Matsunaga, T., Tsuchida, S., Yamamoto, H., 2012. Outline and Prospect of Hyperspectral Imager Suite (HISUI). *Journal of The Remote Sensing Society of Japan* 32(5), 289-286. (*in Japanese*)

Tille, P. J., 2006. Soil-landscapes of Western Australia’s range-lands and arid interior. Department of Primary Industries and Re-gional Development, Western Australia, Perth. Report 313. 32.

Whiting M., Li, L., Ustin, S. L., 2003. Estimating surface soil moisture in simulated AVIRIS spectra, *Proceedings of the 12th JPL Airborne Earth Science Workshop*